AD-A248 701

TECHNICAL REPORT NO. 4

To

The Office of Naval Research
Contract No. N00014-91-J-1414

MECHANISMS OF FRACTURE AND CREEP OF STRUCTURAL ALLOYS

D. A. Koss

Department of Materials Science and Engineering
The Pennsylvania State University
University Park, PA 16802

Annual Report for the period
1 December 1990 - 31 December 1991

REPORT DOCUMENTATION PAGE

Form Approved
OMB No. 0704-0188

1. AGENCY USE ONLY (Leave blank)	2. REPORT DATE March 30, 1992	3. REPORT TYPE AND DATES COVERED Annual Report: 12/1/90 - 12/31/91

4. TITLE AND SUBTITLE
Mechanisms of Fracture and Creep of Structural Alloys

5. FUNDING NUMBERS

6. AUTHOR(S)
D. A. Koss

7. PERFORMING ORGANIZATION NAME(S) AND ADDRESS(ES)
Department of Materials Science and Engineering
Penn State University
University Park, PA 16802

8. PERFORMING ORGANIZATION REPORT NUMBER
Report No. 4

9. SPONSORING/MONITORING AGENCY NAME(S) AND ADDRESS(ES)
Office of Naval Research
800 N. Quincy Street
Arlington, VA

10. SPONSORING/MONITORING AGENCY REPORT NUMBER

11. SUPPLEMENTARY NOTES

12a. DISTRIBUTION/AVAILABILITY STATEMENT
Distribution of this document is unlimited.

12b. DISTRIBUTION CODE

13. ABSTRACT (Maximum 200 words)

Progress is reviewed for a research program which focuses on two aspects which limit the performance of structural alloys. First, in a study generic to a wide range of materials, we are determining the mechanisms, as well as local failure criteria, by which voids or pores grow and link during ductile fracture due to damage accumulation. Secondly, in a study focused specifically at high temperature titanium alloys, we are examining the elevated temperature strength and deformation behavior of a novel, age-hardenable beta titanium alloy. Progress for the period December 1, 1990 to December 31, 1991 is reviewed for the following projects:

(1) modeling the effects of stress state on void linking,
(2) three-dimensional void growth and linking during ductile fracture, and
(3) elevated temperature behavior of a novel age-hardenable beta titanium alloy.

14. SUBJECT TERMS
Tensile Fracture, Damage Accumulation, Void Linking, Beta Ti Alloys, Age-Hardening, Creep, Oxidation

15. NUMBER OF PAGES
22

16. PRICE CODE

17. SECURITY CLASSIFICATION OF REPORT	18. SECURITY CLASSIFICATION OF THIS PAGE	19. SECURITY CLASSIFICATION OF ABSTRACT	20. LIMITATION OF ABSTRACT

NSN 7540-01-280-5500

INTRODUCTION

The performance of advanced structural systems places stringent demands on the strength and fracture resistance of the component materials. One approach to improved system performance is to seek more effective use of existing materials. For example, the use of on-line sensors will enable improved control of dynamic systems to achieve high performance with increased reliability and component durability. Such an intelligent control approach can be successful only if the structural components exhibit a high degree of predictability and the real-time damage accumulation can be predicted under a range of service conditions. The present program addresses one aspect of structural system performance by studying damage accumulation during the tensile fracture of structural alloys. This is being done by a combination of experimental modeling and computational analysis establishing the mechanisms, as well as local failure criteria, by which void or pores grow and link during ductile, microvoid fracture. The results of this study should not only provide a basis for accurate intelligent control of a structural system but also establish improved guidelines for materials processing and design. The effort requires an *integration of materials and mechanics* efforts and relies on the active participation of Dr's. Peter Matic of the Naval Research Laboratory and Michael Stout of the Los Alamos National Laboratory. Two graduate students are currently involved in this aspect of the research program: Andy Geltmacher, a Ph.D. candidate, who is working with Dr. Matic at NRL at the time of this writing, and Luis Forero, a Fulbright Scholar who is on the faculty of University of Industrial de Santander in Columbia, South America.

The second aspect of the present research program recognizes that most commercial beta Ti alloys are age hardenable due to the formation of hcp alpha-phase particles in the 450°-500°C range. Thus, the use of existing beta Ti alloys in a strengthened condition is necessarily limited to relatively low temperatures. As part of this research program, we have recently shown for the first time ever that it is possible to age harden the beta Ti alloy Ti-23-Nb-11Al (at %) with ordered alpha-two precipitates based on Ti_3Al. Hardness data indicate that it is possible to age harden the alloy at temperatures as high as 675°C or ~200°C higher than is possible with conventional alloys. Furthermore, the room temperature yield stresses of specimens aged to peak hardnesses are quite

impressive; yield strengths of 1300 MPa have been obtained for specimens aged at 575°C. The source of the hardening is the formation of ordered alpha-two precipitates with lath-like morphology and which obey a Burger's orientation relationship with the matrix.

The purpose of this aspect of the present investigation is to examine the elevated temperature strength and deformation behavior of the Ti-23Nb-11Al alloy in the 500°-650°C range. Given the importance of oxidation behavior in a service environment in this range, we have also briefly explored the oxidation response in air at 600°-700°C. This research is being conducted by Dana Goto, a M.S. candidate from the University of California at Santa Barbara.

A significant impact of this research is the educational experience derived by the graduate students involved. In addition to Mss'rs. Geltmacher, Forero, and Goto, during 1991 this program also supported Kevin Zeik (Ph.D., May) and Louis Quattrocchi (M.S., May). Kevin is with U.S. Steel and Lou is one of few to be hired last year by Pratt and Whitney. The following sections describe our progress during 1991.

1. Modeling the Effects of Stress State on Void Linking [with Andrew Geltmacher, Ph.D. candidate, Dr. Peter Matic, Naval Research Laboratory, and Dr. Mike Stout, Los Alamos National Laboratory].

The purpose of this research project is to examine the mechanisms by which the stress state influences void linking during damage-controlled, ductile fracture. Previous experiments have shown that the strain to failure normally decreases as the triaxiality of the stress state increases [1-5]. It is also well known that damage-controlled ductile fracture usually has three stages: 1) void nucleation, 2) void growth, and 3) void linking. The effect of stress state on both void nucleation and void growth has been previously established on an experimental basis. For example, the strain to nucleate voids has been shown to decrease as the triaxiality of the stress state increases [2,5-8], while other studies have shown that the growth rate of voids increases as the triaxiality increases [1,5,9]. In contrast, the effect of stress state on void linking has not been established.

The present study examines the effect of stress state on the process of void linking using both experimental and computational analyses. Our approach relies on modeling the three-dimensional

void/pore arrays as two-dimensional arrays of through-thickness holes in sheet (or in some instances plate) material examined in either uniaxial or equal-biaxial tension. Experimentally, panels containing "pseudo"-random arrays of holes are deformed to failure in either uniaxial or equal-biaxial tension in order to observe the effect of stress state on hole linking for a given spatial distribution of holes (i.e., hole "microstructure"). In order to establish the criterion for hole linking, the flow localization and failure behavior of ligaments between pairs of holes have also been examined in specimens tested in either uniaxial tension or equal-biaxial tension. When combined with finite element (FEM) computations, these results will serve to establish not only the criterion which controls ligament failure but also serve to establish multiaxial failure criteria. Subsequent FEM analyses of multi-hole arrays should establish the critical characteristics of the local stress, strain, strain-energy densities within arrays of holes as a function of stress state and microstructure. Taken together, the experimental results and computational analysis should identify both the character and the mechanisms responsible for the influence of stress state on the void/pore linking during low temperature, damage-controlled ductile fracture. This is information critical for any successful damage prediction capability in an intelligent control system.

The model material selected in the present study is 3003 aluminum (1.2Mn-0.12Cu-remainder Al) sheet, which was annealed at 350°C for 2 hours followed by an air cool. The strain hardening exponent, n ($n = d \ln \sigma / d \ln \varepsilon$), has an intermediate value of 0.27 for this condition. In the first part of the study, "pseudo"-random arrays of 63 holes, each with a 1.6 mm diameter, were machined into 254 x 254 mm square sheets using a numerical drilling machine. The specimens were gridded so that the strains in the ligaments between adjacent holes could be measured. It should be noted that the hole arrays are "pseudo"-random in that they are constrained by a minimum allowable hole spacing in which once a hole is present no other hole is allowed. The effect of hole clustering can be examined by generating arrays with two different values of the minimum allowable hole spacing; specifically, the degree of hole clustering increases as the minimum allowable hole spacing decreases.

Equal-biaxial tension testing of specimens containing the arrays of holes were performed at Los Alamos National Laboratories using a MTS hydraulic bulge test machine and large panels so that the regions of the test specimens containing holes were indeed in equal biaxial tension. Test blanks confirmed this stress state. Uniaxial tension was performed on large panels of 3003 aluminum in the H14 condition at ALCOA laboratories for comparison to the equal-biaxial tests. The tests were performed at Alcoa because the panels were too wide any grips available at Penn State.

In addition to establishing the behavior of specimens with arrays of holes, test panels containing hole pairs were studied. Specimens with two 1.6 mm holes spaced 1, 2 and 3 hole diameters apart were examined in both uniaxial and equal-biaxial tension. As in the tests of specimens with hole arrays, the specimens were gridded using a photo resist technique in order that the localization strains could be measured. These data will be used to validate FEM data as well as to establish a strain-based criterion for hole linking.

The experimental results indicate that a principal effect of stress state on hole linking is the directional nature of "hole-linking paths". This is illustrated in Figure 1 which contrasts the localization paths for specimens which have been deformed under either (a) equal-biaxial tension or (b) uniaxial tension. In equal-biaxial tension the localization paths are "multi-directional" in that the applied stress state allows for the localization (and subsequent fracture) of the ligaments between holes to depend only on the spacing between the holes. In contrast, Figure 1b shows that in uniaxial tension the localization paths are constrained to a plane approximately perpendicular to the loading axis. In this case, the linking of the ligaments is dependent on both spacing and orientation of adjacent holes.

The above multidirectionality effect contributes to the important experimental observation that specimen fracture occurs soon after the onset of ligament localization in equal-biaxial tension. In contrast, specimen fracture in uniaxial tension is more gradual with much more macroscopic strain accumulating from the onset of the localization in the first ligament specimen fracture. This suggests the following implication for the damage-induced fracture of structural metals: one effect

of stress state on void linking is that failure is likely to occur soon after the initiation of damage in multiaxial tension while void linking is more gradual in uniaxial tension. This has been shown in previous work for materials without holes for other aluminum alloys [11,12] and titanium sheet [2].

The above observations suggest that in a random distribution of voids, localization between the voids should be easier in equal-biaxial tension due to the "multi-directionality" of the localization paths. In view of previous results indicating the importance of hole clustering on linking in uniaxial tension, [10] we would also expect hole linking to be retarded if minimum interhole spacing is increased and hole clustering decreased. This is shown in Fig. 2 where the average, macroscopic specimen strain needed to promote localization increases as the spacing between holes increases. Examination of Figure 2 also shows that strain localization occurs under conditions approaching plane strain even though the applied strain path is equal-biaxial.

Experiments involving specimens containing pairs of holes have been deformed in either uniaxial or equal-biaxial tension in order to examine the effect of stress state on the linking criteria. As shown in Figure 3, which indicates the strains measured in the ligament between the holes at the onset of localization for both applied stress states, strain localization within the ligaments (a) occurs under conditions of nearly plane strain for both applied stress states, and (b) appears to obey two different critical thickness strain criteria for uniaxial and equal-biaxial tension. The critical strain value for ligament localization is less in uniaxial tension than in equal-biaxial tension. Thus, the data indicate that the applied uniaxial tension allows for the plane-strain conditions to be achieved earlier in the deformation process; as a result, the critical thickness strain is lower. It was also noted that the critical thickness strain is not dependent on the orientation of the ligament with respect to the rolling direction for this material.

Our results also indicate that the applied macroscopic strain required to trigger localization within the ligaments increases as interhole spacing increases; see Fig. 4. This is expected from previous studies and is a principal reason why clusters of voids or high void contents promote fracture. However, Figure 4 indicates two somewhat surprising observations: (a) the

macroscopic strain to trigger flow localization and ligament fracture in equal biaxial not only exceeds that in uniaxial tension, but (b) it is also much more sensitive to interhole spacing. This implies that avoiding void clustering may be quite important in delaying void linking and avoiding fracture under multiaxial loading conditions.

In summary, our modeling indicates that the effect of stress state on hole/void linking depends on the competition between the influence of stress state on (a) hole-linking strains required to trigger flow localization between holes (such strains which increase with increasing biaxiality and interhole spacing) and (2) the "multi-directionality" of the linking paths (which also increases with increasing biaxiality). The latter promotes linking in equal biaxial tension while the former retards it. Thus, it is conceivable to us that a material with a microstructure consisting of uniformly spaced particles (no void clustering) and exhibiting a high level of strain hardening (inherently resistent to plastic localization) will show better fracture resistance in multiaxial tension than in uniaxial tension, assuming identical void nucleation behavior.

Future efforts involve the use of finite element modeling techniques to determine why some of the above behavior occurs and how to extend these observations in a predictive manner to other materials. Presently we are modeling the pair-of-holes experiments. The work will then be expanded to examine multiple-hole arrays studied by both computer simulation and experiments.

2. Three-Dimensional Void Growth and Linking During Ductile Fracture
[with Luis Forero, M.S. candidate]

While two-dimensional modeling and analysis can provide the framework for predicting the fracture of structural materials, an accurate constituitive relationship must be based on a three-dimensional (3D) analysis. However, a realistic 3D model capable of predicting the tensile fracture of porous or voided metals requires (a) a description of the 3D distribution, shape, and size of the voids or pores (progress in this aspect has been made using cell approaches), (b) local strains or strain-energy densities distributions near voids, (c) the associated void growth behavior, especially in the presence of neighboring voids, and (d) a valid failure criterion for the linking of voids. Current analyses still tend to use a cavity growth relationship developed for an isolated void

embedded in a non-hardening matrix [9]. This ignores the influences of strain hardening, strain-rate hardening, and the presence of neighboring voids. The latter factor should be especially important at high volume fractions of voids; this should be the case in the latter stages of damage accumulation or the fracture of materials containing large volume fractions of void-nucleating particles, such as in particulate-reinforced MMC's. Thus, fracture analyses continue to utilize void growth analyses which are likely to be inaccurate, especially at large volume fractions of voids. Furthermore, there is no adequate criterion for void linking. The most commonly used criterion was a simple geometric argument based on a void size-to-spacing ratio [13,14], and this has been shown to be inadequate [6].

The present research project has been recently initiated as an effort (a) to determine the growth behavior of isolated as well as neighboring voids and (b) to establish the conditions for void linking. At this time, the study is experimental in nature; we anticipate computational analyses to compliment these observations. The present project is based on modeling three-dimensional coplanar arrays of cavities by pairs of triplets of cavities. Tensile specimens containing nearly spherical internal cavities have been made by diffusion bonding of pure 18 mm diameter titanium bar at 695°C, 29 MPa pressure for 150 minutes. The 1.2 mm diameter cavities were introduced by drilling one end face of the cylinders, which produced a cylindrical cavity with a semi-spherical bottom. During diffusion bonding, the shape of the cavities changed to near spherical void due to effect of the compression load and diffusion. Initial tests are being conducted on tensile specimens with pairs of 1.2 mm diameter cavities roughly one cavity diameter apart. The cavities are centrally located in a gauge section with square 10x10 mm cross section. This specimen geometry permits the monitoring of cavity growth and linking by interrupting the tensile tests and examining the cavity dimensions generating an ultrasonic C-scan image with a 15 MH_Z transducer.

Figure 5 shows a C-scan image of the pair of internal cavities initially spaced 0.7 x hole diameter apart and subjected to uniaxial tensile deformation. As can be clearly seen, deformation causes strain-induced void growth with void extension both parallel to and transverse to the tensile

axis. The latter is unexpected since theory for the growth of isolated voids predicts a strain-induced contraction of the void in the transverse dimension.

The above trends are confirmed in Figure 6 where tensile tests have been interrupted to obtain C-scan images in order to measure cavity growth as a function of macroscopic strain. As can be seen in Figure 6, there is sustained cavity growth in both the longitudinal and transverse directions. In fact, the data suggest that the rate of transverse growth may in fact exceed that measured longitudinally, parallel to the tensile axis. Such transverse void growth must be induced from interactive effects from the neighboring void. It results in a strain-induced necking of the inter-cavity ligament at a strain of ≈0.20, as shown in Figure 6. Interestingly, preliminary data (two tests) suggest a "plateau" in the rate of ligament necking occurring at strains of ≅ 0.05 to 0.10, with accelerated necking thereafter. This would be consistent with a load instability and accelerated necking of the ligament, but the reproducibility of such data must be established.

We may summarize these initial data by the following observations:

(1) it is possible to fabricate test specimens by diffusion bonding titanium rods to contain nearly spherical internal cavities such strain-induced cavity growth and linking can be determined using ultrasonic imaging. Both the number and spatial orientation of the cavities can be controlled, but initial experiments will be confined to single, pairs, or triplets of cavities..

(2) during deformation, closely spaced cavities (spacing ≅ 0.7 cavity diameter) exhibit strong interaction effects resulting in a rate of transverse cavity growth which is equal to or slightly greater than longitudinal cavity growth;

(3) cavity linking occurs by a ligament necking process which may include a plastic instability process within the ligament resulting in accelerated ligament necking. We expect this process to be very sensitive to the spacing between voids and the strain hardening of the matrix.

Future work will be directed at four simple arrays shown below which explore (a) the effect of intercavity spacing (configuration 1 and 2), (b) the effect of pairs of neighboring cavities on the

growth of a third cavity (configuration 3), and (c) comparative growth behavior of a single vs. pairs of cavities (configuration 4).

Configuration	# Voids	Scheme
1	2	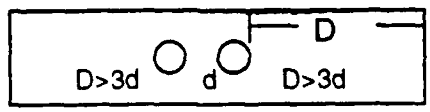
2	2	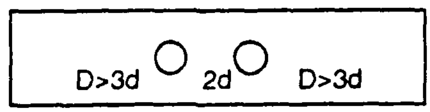
3	3	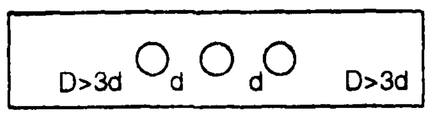
4	3	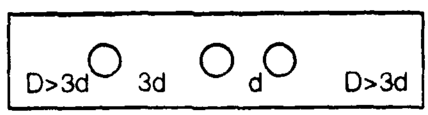

Figure 7. A schematic illustrating proposed cavity configurations for future research.

3. <u>Elevated Temperature Behavior of an Age-Hardenable Beta Titanium Alloy</u>
[with Dana Goto, M.S. candidate]

Metastable bcc beta titanium (β-Ti) alloys, although possessing good low temperature ductility in the solution-treated condition and high strength levels in the aged condition, usually exhibit poor elevated temperature mechanical properties. This poor resistance to elevated temperature deformation appears to be related to the anomalously high rate of self-diffusion in unalloyed bcc titanium [15]. As a result, existing β-Ti alloys have been observed to strain soften under elevated temperature mechanical testing conditions, suggesting processes involving recovery offset those of hardening [16].

The purpose of the current work is to address the elevated temperature deformation mechanisms in a novel β-Ti alloy strengthened by the formation of alpha-two precipitates based on

Ti_3Al. The alloy being studied has a nominal composition Ti-23Nb-11Al (in atomic %) and is characterized by a pronounced age hardening response and increase in room temperature compressive strength [16]. Of particular significance is that the precipitation hardening occurs at temperatures up to 675°C, or about 200°C higher than conventional beta Ti alloys. The current study explores the elevated temperature behavior of the Ti-23Nb-11Al (Ti-23-11) alloy.

The Ti–23–11 alloy is being mechanically tested between the temperatures of 550°C and 650°C. This temperature range was chosen as the probable maximum application temperature range for this alloy in its desirable heat-treated conditions. All tests are performed using compression tests over a range of strain rates ($10^{-4}s^{-1} < \dot{\varepsilon} < 10^{-2}s^{-1}$) on samples in selected heat-treated conditions. Prior to testing, all samples received a solution heat treatment at 1000°C for 1 hour and water quenched. Subsequent to this heat treatment, samples were divided into three aging treatments: (1) 575°C for 6 hours (denoted as "575/6"), (2) 625°C for 6 hours, or (3) a 675°C for 2 hours.

Figure 8 shows the presence of strain softening in a sample in the 675°C for 2 hours heat-treated condition. Strain softening, as previously mentioned, indicates that recovery processes dominate over hardening processes. Since creep deformation occurs at the balance of recovery and hardening process, results such as those in Figure 8 suggest that at 638°C the Ti-23-11 alloy is susceptible to creep deformation. If this is the case, then strain-rate hardening should become pronounced and a creep stress exponent approaching a value of about five might be observed. Strain-rate jump tests have been performed to determine the creep stress exponents over a range of temperatures; see Figure 9. The large stress exponents $n = (d\ln\dot{\varepsilon}/d\ln\sigma) \simeq 13+$ suggest that, while not in a steady-state dislocation creep regime, the Ti-23-11 alloy exhibits creep-assisted deformation, especially at 638°C and $10^{-4}s^{-1}$ strain rate.

An off-shoot of the current work being investigated is the possibility of enhancing room temperature ductility by a step-aging process of the current bcc beta titanium alloy. Hida and Weissmann found that a two-step aging heat treatment yielded a significant increase in ductility by altering the dislocation movement path [17]. While the Ti-23Nb-11Al has good room temperature

ductility in the solution heat-treated condition (≈20%), in the peak-hardness precipitation heat-treated condition (aged 575°C/6 hrs), its ductility decreases dramatically (<1%). In the "conventional" precipitation heat-treated condition, under-aging yields small shearable precipitates a very coarse planar in the matrix; over-aging yields large grain boundary precipitates but fine uniform slip within the grains. Thus the goal is to induce the fine, uniform slip caused by particle looping but without extensive grain boundary precipitation causing intergranular fracture. Thus we have designed a duplex heat treatment (DHT). The goal of the duplex heat treatment is to precipitate a uniform distribution of matrix precipitates which are large enough to induce dislocation looping or climbing rather than shearing, and to suppress discontinuous precipitation on grain boundaries. Using uniform slip as an indicator of particle looping, a preliminary DHT study has identified the optimal DHT to be an initial 375°C for 24 hours followed by a subsequent heat treatment of 675°C for 8 hours. The methodology was based on the observation that a low temperature precipitation heat treatment causes a fine uniform distribution of matrix precipitates. A subsequent higher temperature age coarsens these precipitates with hopefully little of no discontinuous grain boundary precipitation; this confirmed by optical microscopy. Tensile specimens are currently being machined to test influence of the above heat treatment on ductility.

In addition to elevated temperature mechanical tests, oxidation experiments were performed in air between 600°C and 700°C in a thermogravimetric analysis (TGA) unit. Since oxidation of titanium involves processes which are diffusion controlled, the TGA data indicate that during oxidation, the specimen weight increases parabolically with time. Therefore weight gain may be represented by the general rate equation for parabolic oxidation kinetics

$$m^2 = k_p t \tag{1}$$

where m is the weight gain per unit area of sample, k_p is the parabolic rate constant, and t is the time of exposure at the oxidation condition. The parabolic rate constant corresponding to a particular oxidation temperature may be represented by the Arrhenius relationship

$$k_p = k_o \exp(-Q/RT) \tag{2}$$

where k_o is the preexponential factor, Q is the effective activation energy of the rate limiting oxidation process, R is the gas constant, and T is the absolute oxidation temperature. Plotting the parabolic rate constants as a function of temperature allows the calculation of an apparent activation energy of the oxidation process.

From weight gain histories, illustrated in Figure 9, parabolic rate constants were determined and the apparent activation energy for Ti-23Nb-11Al oxidation was calculated. The calculated activation energy of 239 kJ mol^{-1} coincides with literature values for oxygen diffusion in titanium [18]. Visual inspection of oxidized surfaces revealed entire blackened surfaces, with scattered patches of an off-white scale which were identified as TiO_2 by x-ray diffraction (XRD). The black surface scale was not identified due to an insufficient quantity present to obtain an identifiable signal. Due to the absence of a continuous oxide scale, oxidation appeared rate limited by oxygen dissolution into the metal. TiO_2, although present, was not a continuous scale over the entire oxidized surface. Therefore scale formation probably did not contribute greatly to the oxidation process.

The absence of an oxide scale may be explained by the non-establishment of an oxygen-saturated near-surface region. Wallwork and Jenkins postulated scale formation on titanium oxidized in pure oxygen over the temperature range of 800°C to 1000°C probably proceeded oxygen saturation of near surface material [19]. XRD results of the current alloy suggest near-surface material was not saturated with oxygen due to the presence of an oxygen concentration gradient, as observed by compositional broadening [20]. The presence of an oxygen concentration gradient in the material also implies the oxygen transport rate from the surface region to the bulk exceeded the oxygen absorption rate into the metal. Although the oxidation of Ti-23Nb-11Al in air, over the temperature range of 600°C to 700°C, does not produce a protective oxide scale as observed by the continuous weight gain during exposure, this alloy is an improvement over unalloyed titanium and the metastable β-Ti alloy, Beta21S; see Figure 10.

REFERENCES

1) J.W. Hancock and A.C. Mackenzie, J Mech Phys Solids, 24, 147 (1976).

2) R.J. Bourcier and D.A. Koss, Acta Metall, 32, No. 11, 2091 (1984).

3) F. Yunchang and D.A. Koss, Met Trans A, 16A, 675 (1985).

4) D. Kwon and R.J. Asaro, Acta Metall, 38, No. 8, 1595 (1990).

5) D. Kwon and R.J. Asaro, Met Trans A, 21A, 117 (1990).

6) S.H. Goods and L.M. Brown, Acta Metall, 27, 1 (1979).

7) A. Needleman, J App Mech, 54, 525 (1987).

8) D. Kwon, Scripta Met, 22, 1161 (1988).

9) J.R. Rice and D.M. Tracey, J Mech Phys Solids, 17, 201 (1969).

10) P. E. Magnusen, D. A. Koss, and E. M. Dubensky, Acta Metall., 36, 1503 (1988).

11) G. LeRoy and J.D. Embury, in Formability - Analysis, Modeling and Experimentation, eds. S.S. Hecker, A.K. Ghosh and H.L. Gegel, The Metallurgy Society of AIME, 1978, pp. 183-207.

12) R. Sowerby and B.K. Sareen, in Formability Topics - Metallic Materials, eds. B.A. Niemeier, A.K. Schmieder and J.R. Newby, American Society for Testing and Materials, 1975, pp. 49-64.

13) L. M. Brown and J. D. Embury in Proc. 3rd Int. Conf. on Strength of Metals and Alloys, 1973, p. 164.

14) G. LeRoy, J. D. Embury, G. Edward, and M. F. Ashby, Acta Metall., 29, 1509 (1981).

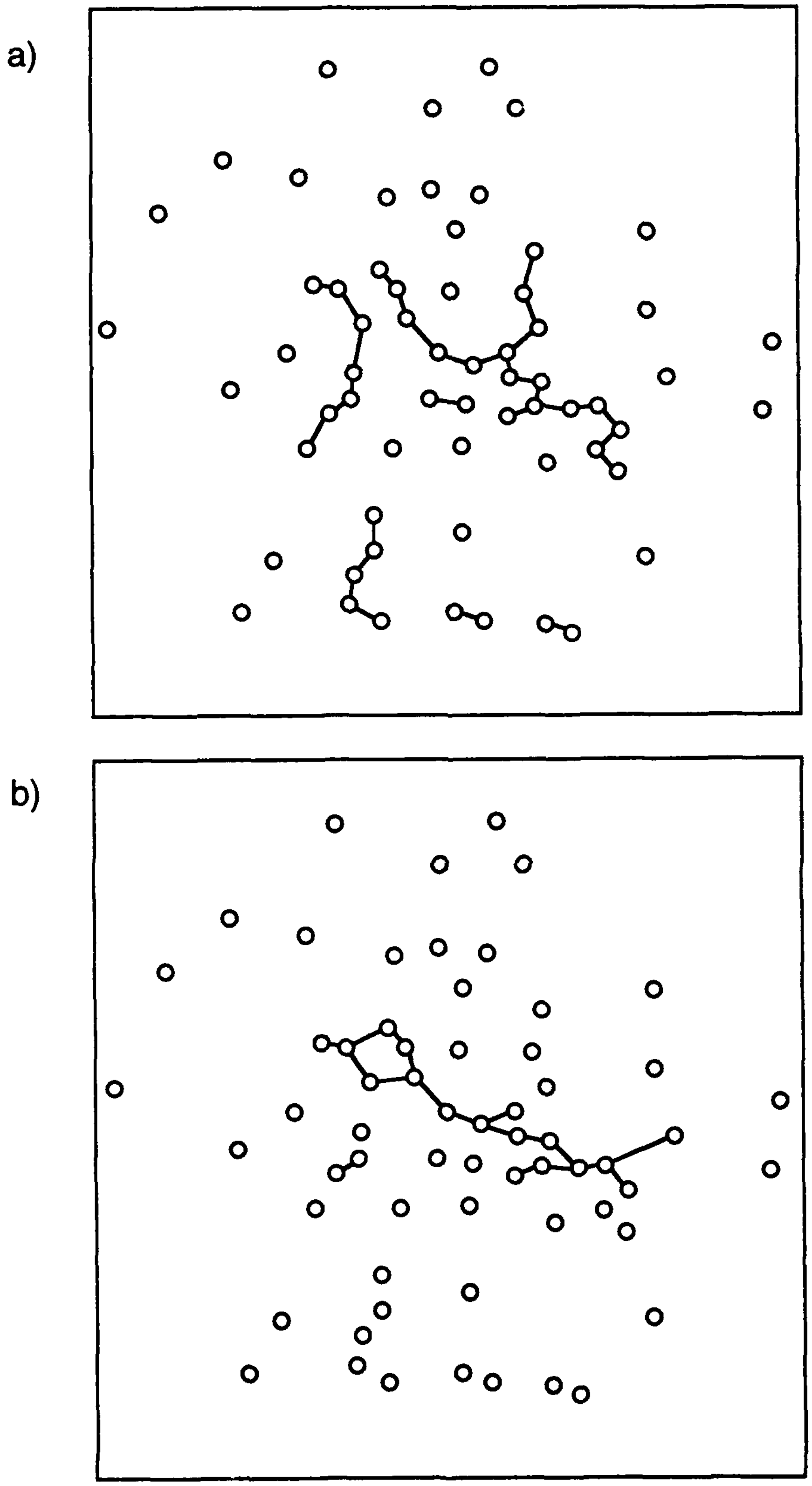

Figure 1: Schematic diagram of the localization paths developed in specimens with a minimum allowable hole spacing of 1.6 mm tested in either a) equal-biaxial tension or b) uniaxial tension. *The tensile axis is vertical for the uniaxial case.*

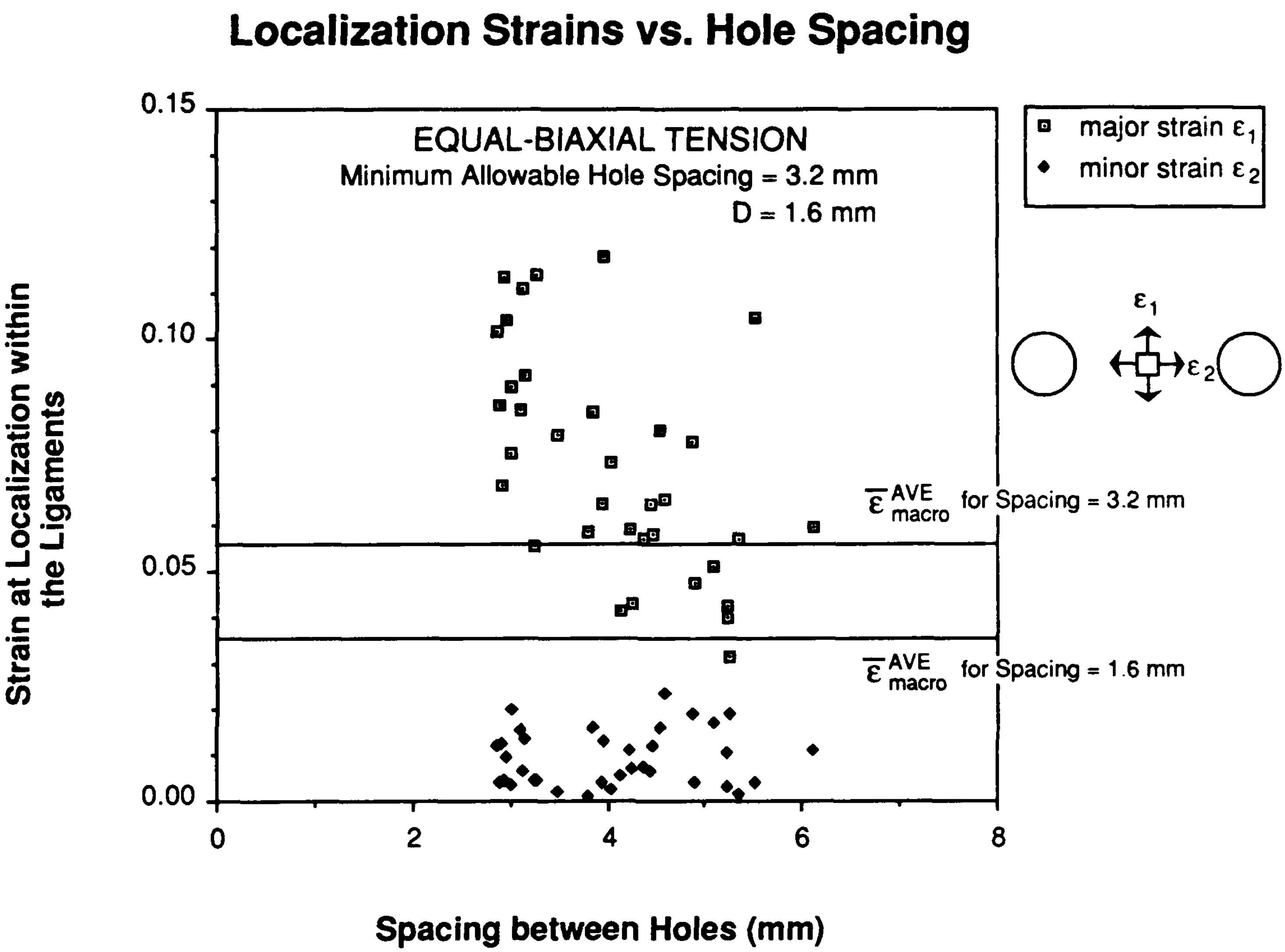

Figure 2: The dependence of the major and minor principal strains within the ligaments at localization as a function of interhole spacing for a "pseudo"-random array of 1.6 mm holes characterized by a minimum allowable hole spacing of 3.2 mm. The macroscopic, effective strains are also shown for specimens with both minimum allowable hole spacings used in the study.

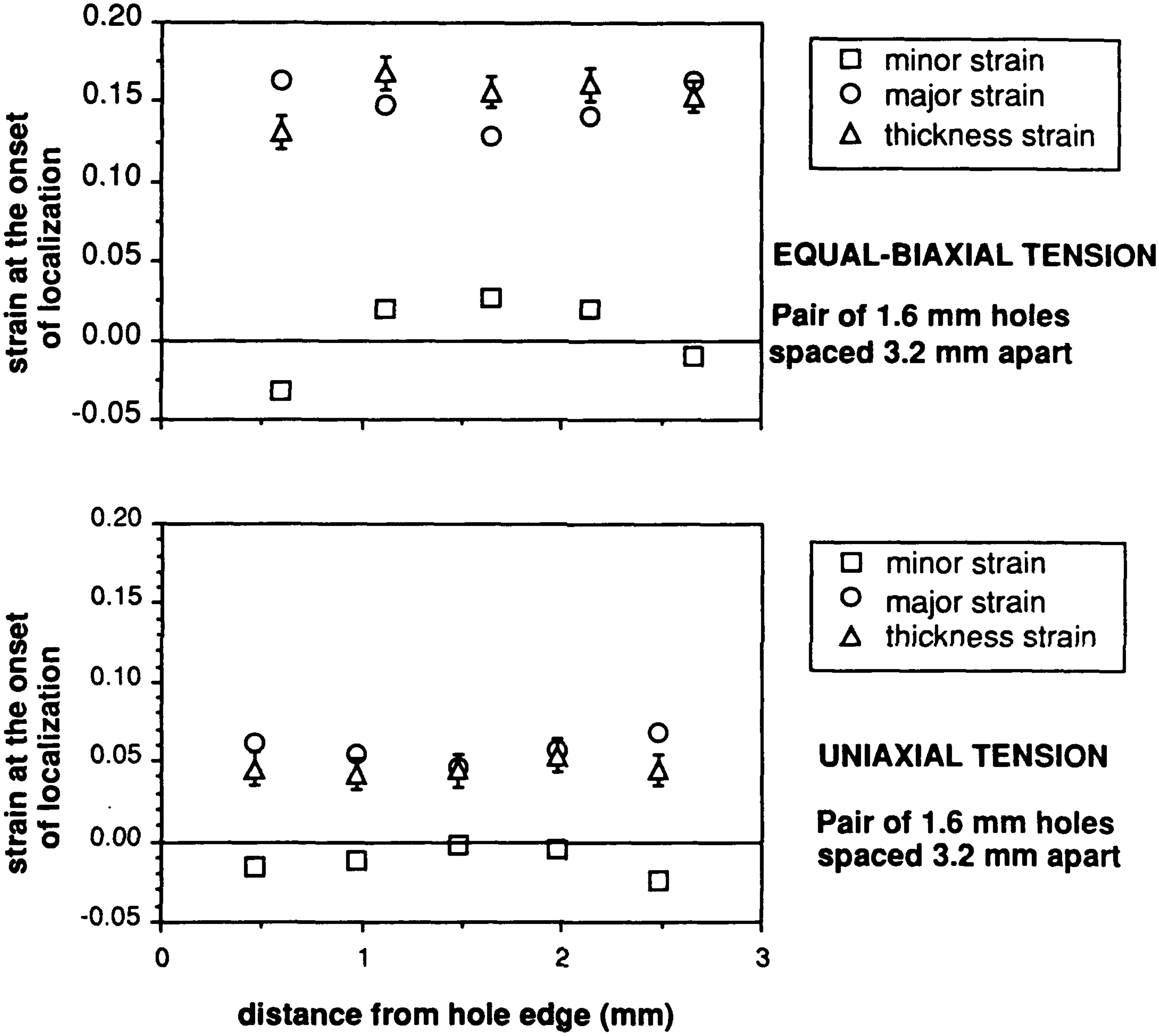

Figure 3: The dependence of the local principal strain components at the onset of ligament localization as a function of the distance from the hole edge for specimens tested in either uniaxial or equal-biaxial tension.

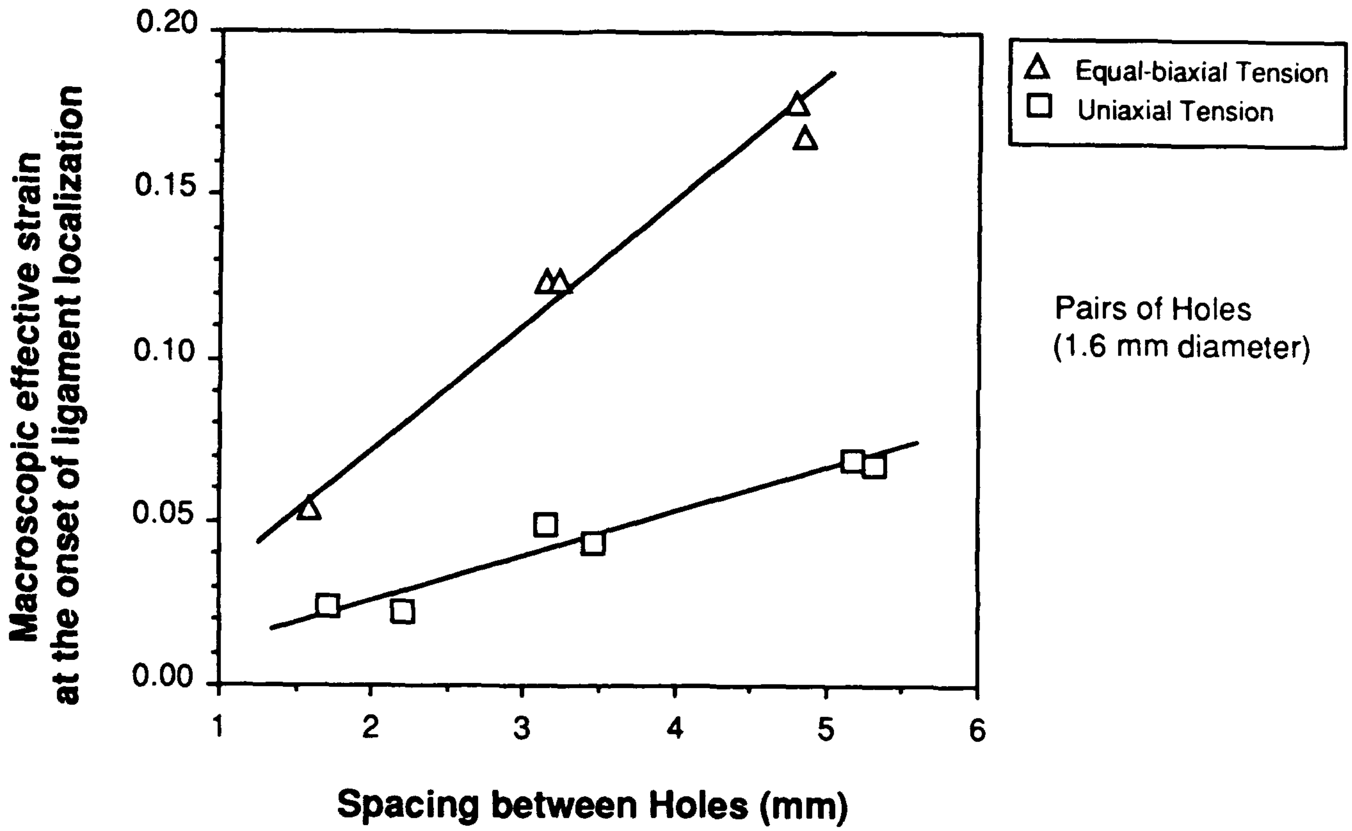

Figure 4: The dependence of the macroscopic, effective strain at the onset of ligament localization on the spacing between holes. Data is shown for both uniaxial and equal-biaxial tension.

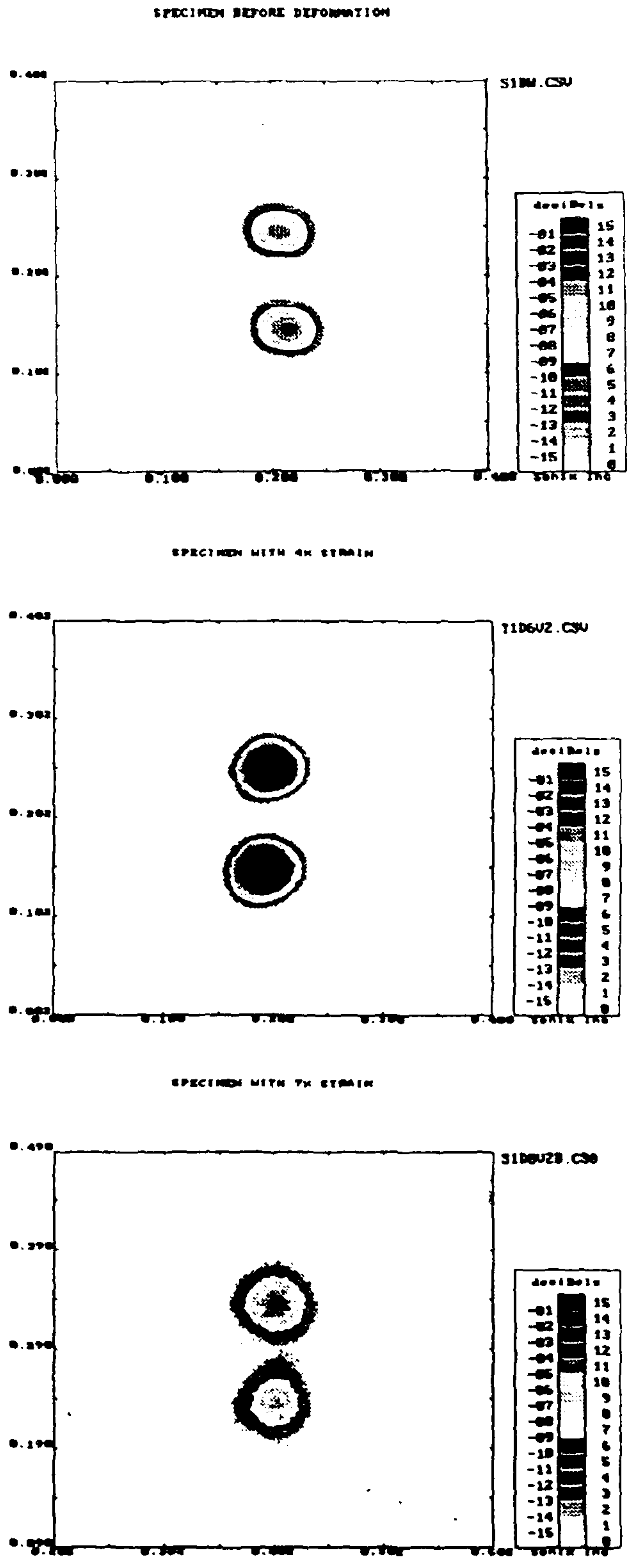

Figure 5. Ultrasonic scan images of two internal cavities within a tensile specimen (a) initially, (b) after 4% strain, and (c) after 7% strain.

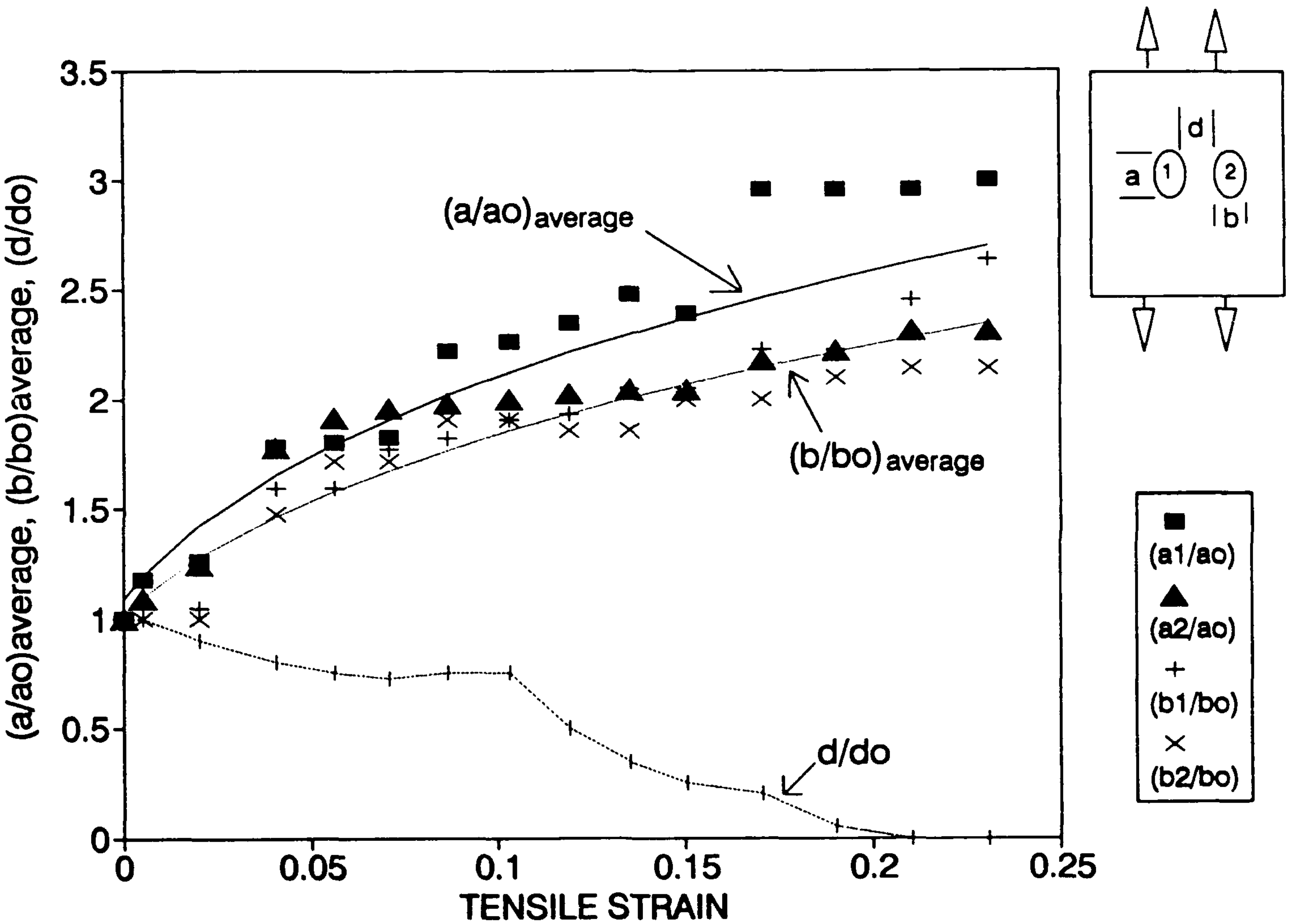

Figure 6. The effect of increasing plastic strain on the principal diameters (a,b) of an initially spherical void ($a_0=b_0=c_0$) and on spacing ligament (d) between voids with an initially intervoid spacing (d_0). The solid and dot lines represent the fitted curves of the average values "a/a_0 and b/b_0" respectively.

THIS

PAGE

IS

MISSING

IN

ORIGINAL

DOCUMENT

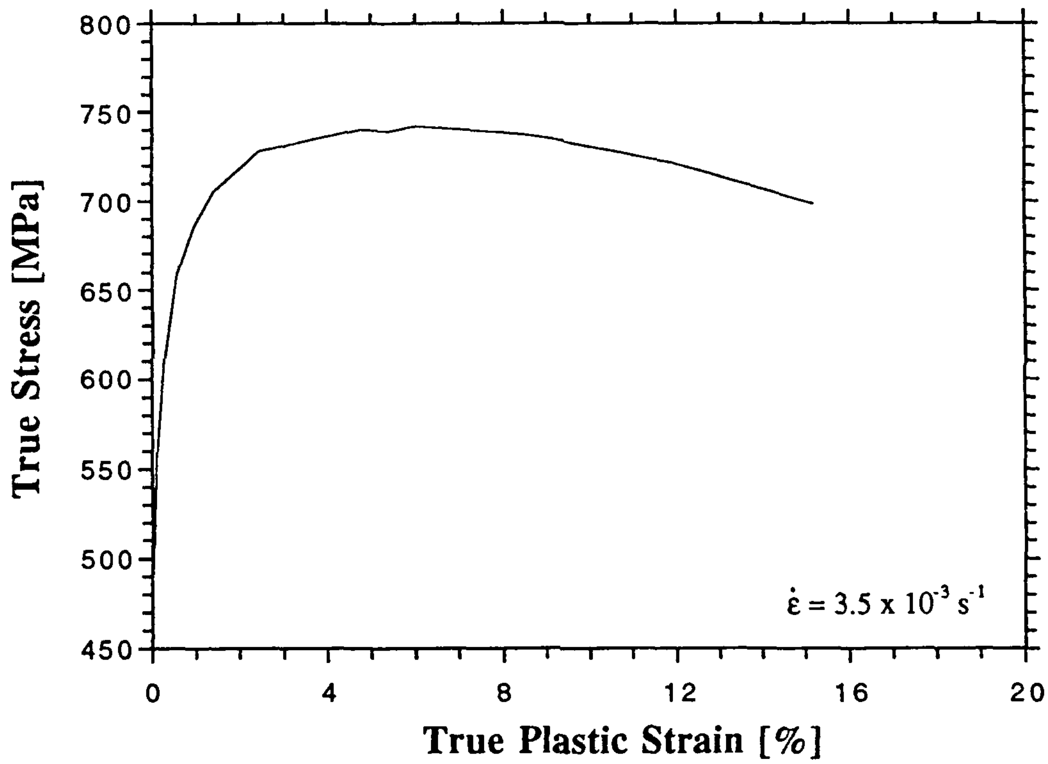

Figure 8. True stress-true strain response of the Ti-23Nb-11Al alloy tested in the 675°C / 2 hours condition. Deformation was in slow strain rate compression ($3.5 \times 10^{-3}\ s^{-1}$) at 638°C.

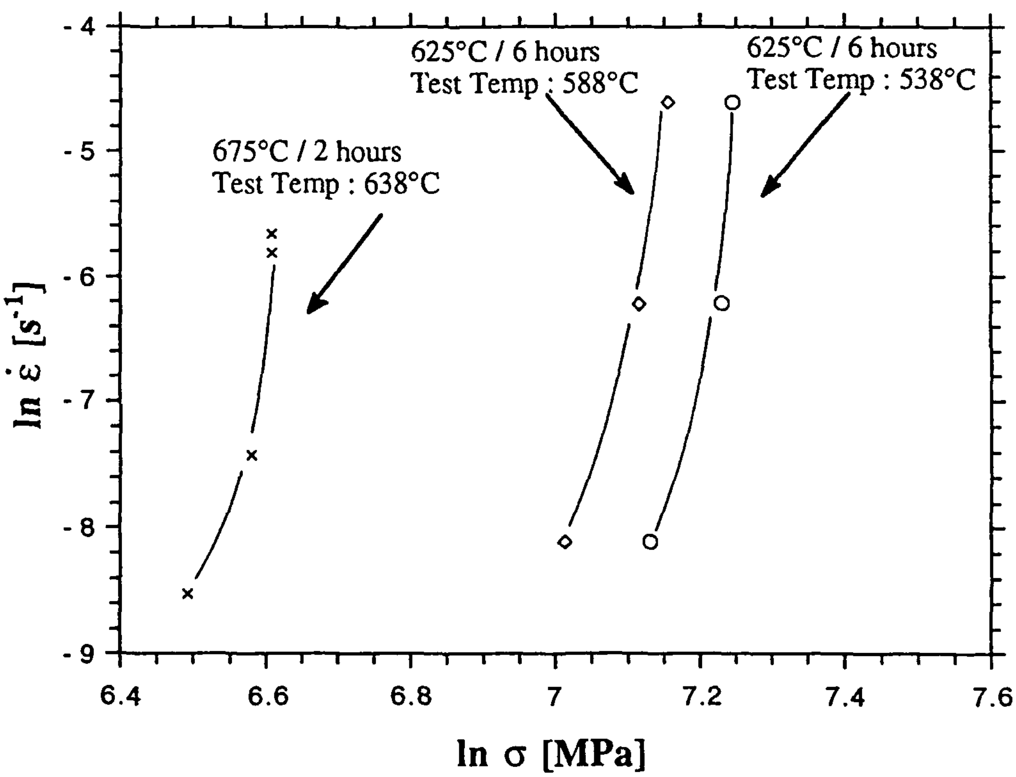

Figure 9. Summary of initial elevated compression tests. Illustrated are results from a sample in the 675°C / 2 hours condition, and two in the 625°C / 6 hours condition tested at 638°C, 588°C and 538°C, respectively.

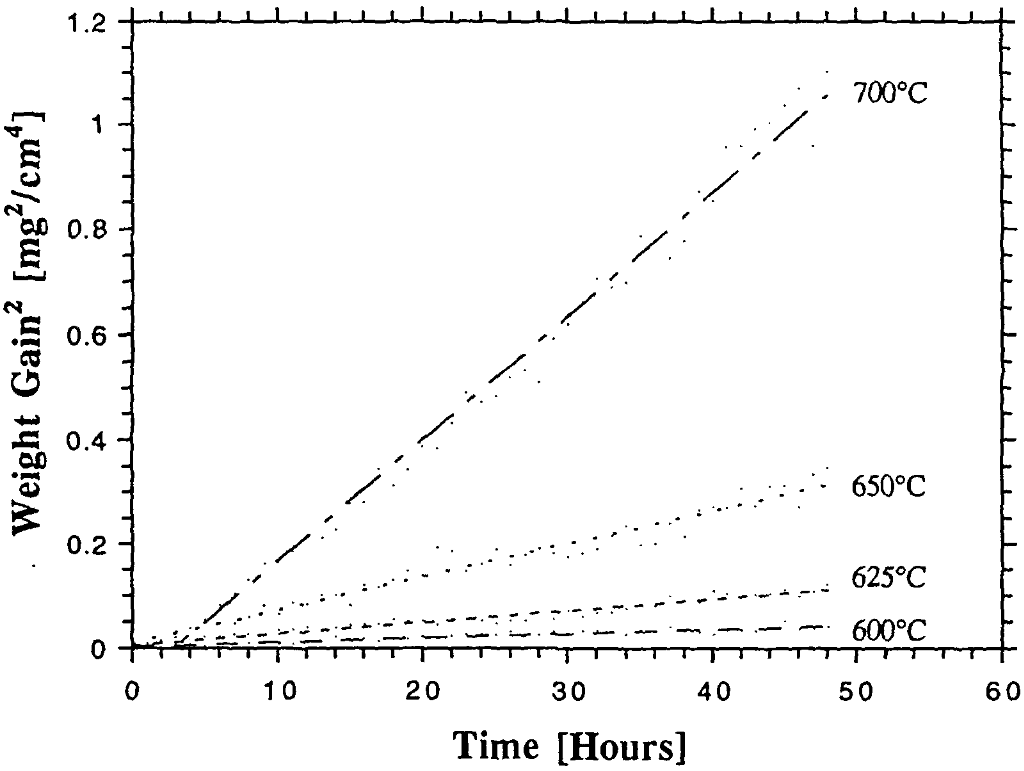

Figure 10. TGA results of Ti-23Nb-11Al oxidized in air for 48 hours between 600°C and 700°C. Note curve is plotted in parabolic coordinates; i.e. weight gain^2 vs. time.

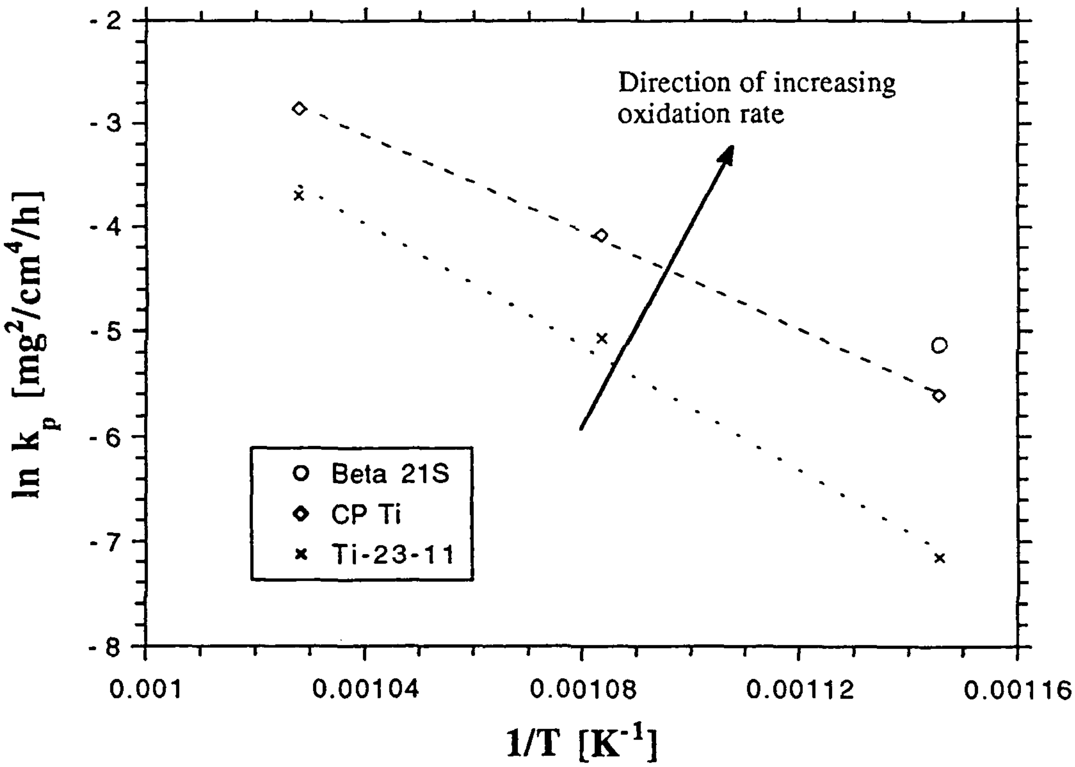

Figure 11. Arrhenius plot of parabolic rate constants of Beta21S, CP Ti, and Ti-23Nb-11Al. Note: Slopes yield the apparent activation energy for oxidation.